Experimental and Theoretical Investigations of the Effect of Deprotonation on Electronic Spectra and Reversible Potentials of Photovoltaic Sensitizers: Deprotonation of *cis*-L_2RuX_2 (L = 2,2′-Bipyridine-4,4′-dicarboxylic Acid; X = CN^-, NCS^-) by Electrochemical Reduction at Platinum Electrodes

Georg Wolfbauer, Alan M. Bond,* Glen B. Deacon, Douglas R. MacFarlane,* and Leone Spiccia

Contribution from the Department of Chemistry, Monash University, Clayton 3168, Victoria, Australia

Received July 9, 1999

Abstract: Deprotonation of the photovoltaic dye sensitizers *cis*-$(H_2\text{-dcbpy})_2RuX_2$ (L_2RuX_2) (X= $-CN^-$, $-NCS^-$; H_2-dcbpy = L = 2,2′-bipyridine-4,4′-dicarboxylic acid) can be achieved in dimethylformamide by reductive electrolysis at platinum electrodes at 20 °C, which allows the thermodynamic and spectral changes associated with deprotonation to be established. The overall reaction that occurs when a potential of −2.0 V vs Fc/Fc^+ (Fc = ferrocene) is applied to a platinum electrode can be summarized as $(H_2\text{-dcbpy})_2Ru(NCS)_2 + xe^- \rightarrow [(H_{2-x/2}\text{-dcbpy}^{x/2-})_2Ru(NCS)_2]^{x-} + {}^x/_2H_2$, where x is always slightly less than 4. Thus, under certain experimental conditions, $[(H\text{-dcbpy}^-)_2RuX_2]^{2-}$ is believed to be the major product formed by bulk electrolysis, where H-dcbpy$^-$ is the singly deprotonated H_2-dcbpy ligand. The hydrogen gas formed in this electrochemically induced deprotonation can be generated heterogeneously at the electrode surface or via homogeneous redox reactions between ligand-reduced forms of L_2RuX_2 and protons or water. Short time domains, reduced temperatures, and glassy carbon electrodes lead to detection of transiently stable ligand-reduced forms of L_2RuX_2. The reversible half-wave potentials for the ligand-based reduction of electrochemically generated deprotonated L_2RuX_2 are 0.65 V more negative than their protonated counterparts. In contrast, deprotonation leads to the metal-based oxidation process being shifted by only about 0.3 V. Interestingly, protonated and deprotonated forms of L_2RuX_2 do not coexist in a facile acid−base equilibrium state on the voltammetric time scale. Data obtained from electrogenerated deprotonated forms of the sensitizers are compared to those found for "salts" used in photovoltaic cells which are prepared by reaction of L_2RuX_2 with tetrabutylammonium hydroxide. Molecular orbital calculations were employed to provide theoretical insights into the effect of deprotonation on reversible potentials and electronic spectra, and results are in good agreement with experimentally obtained data. Electronic spectra, measured in situ during the course of reduction in a spectroelectrochemical cell, reveal that all bands shift to higher energies and that the absorbance decreases as deprotonation occurs. Implications of the importance of the findings related to reduction potentials and electronic spectra to the operation of photovoltaic cells that utilize deprotonated forms of sensitizers are considered.

1. Introduction

The electron-transfer and photochemical properties of ruthenium polypyridyl compounds used as sensitizers in photovoltaic cells have been studied extensively for many years. For example, voltammetric techniques have been used to determine reversible potentials[1] associated with oxidation or reduction[2−4] of this class of compound, and spectroscopic studies[5−8] that are related to the strong metal-to-ligand charge-transfer (MLCT) bands that occur in the visible part of the electronic spectrum have been widespread.

Substitution of the bipyridine ligands in the 4,4′ position with carboxylate groups enables these substituted ruthenium polypyridyl compounds to be attached to TiO_2 semiconductor surfaces via ester linkages.[7,9−11] The combination of the light absorptive properties of the chemically attached ruthenium sensitizer and the charge separation properties of the semiconductor electrode enable photoelectrochemical cells to be constructed[12−15] with energy conversion efficiencies of greater

* To whom correspondence should be addressed. E-mail: A.Bond@sci.monash.edu.au; D.MacFarlane@sci.monash.edu.au. Fax: ++61-3-99054597.

(1) Tokel-Takvoryan, N. E.; Hemingway, R. E.; Bard, A. J. *J. Am. Chem. Soc.* **1973**, *95*, 6582−6589.
(2) Keene, F. R.; Salmon, D. J.; Walsh, J. L.; Abruña, H. D.; Meyer, T. J. *Inorg. Chem.* **1980**, *19*, 1896−1903.
(3) Lai, Y. K.; Wong, K. Y. *J. Electroanal. Chem.* **1995**, *380*, 193−200.
(4) Slattery, S. J.; Gokaldas, N.; Mick, T.; Goldsby, K. A. *Inorg. Chem.* **1994**, *33*, 3621−3624.
(5) Pinnick, D. V.; Durham, B. *Inorg. Chem.* **1984**, *23*, 1440−1445.
(6) Heimer, T. A.; Bignozzi, C. A.; Meyer, G. J. *J. Phys. Chem.* **1993**, *97*, 11987−11994.
(7) Argazzi, R.; Bignozzi, C. A.; Heimer, T. A.; Castellano, F. N.; Meyer, G. J. *Inorg. Chem.* **1994**, *33*, 5741−5749.
(8) Juris, A.; Balzani, V.; Barigelletti, F.; Campagna, S.; Belser, P.; Zelewsky, A. *Coord. Chem. Rev.* **1988**, *84*, 85−277.
(9) Meyer, T. J.; Meyer, G. J.; Pfennig, B. W.; Schoonover, J. R.; Timpson, C. J.; Wall, J. F.; Kobusch, C.; Chen, X. H.; Peek, B. M.; Wall, C. G.; Ou, W.; Erickson, B. W.; Bignozzi, C. A. *Inorg. Chem.* **1994**, *33*, 3952−3964.
(10) Murakoshi, K.; Kano, G.; Wada, Y.; Yanagida, S.; Miyazaki, H.; Matsumoto, M.; Murasawa, S. *J. Electroanal. Chem.* **1995**, *396*, 27−34.
(11) Finnie, K. S.; Bartlett, J. R.; Woolfrey, J. L. *Langmuir* **1998**, *14*, 4, 2744−2749.

10.1021/ja992402g CCC: $19.00
Published on Web 12/21/1999

Scheme 1. Simplified Diagram Showing the Transitions That Occur in a Photoelectrochemical Solar Cell[a]

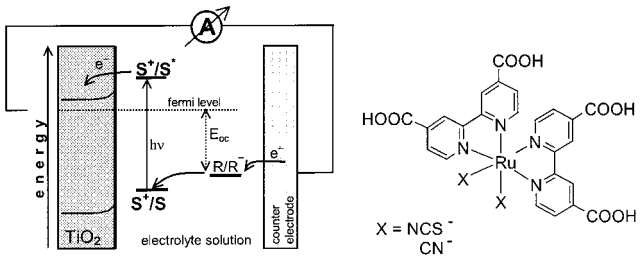

[a] S is the sensitizer (structure, see right), R is the electrolyte (commonly I^-/I_3^-), and E_{oc} is the open circuit potential.

than 10%. The most common sensitizer used in photovoltaic systems of this kind is *cis*-$(H_2\text{-dcbpy})_2Ru(NCS)_2$, which for convenience will also be written as $L_2Ru(NCS)_2$ (H_2-dcbpy = L = 2,2′-bipyridine-4,4′-dicarboxylic acid). This sensitizer provides excellent absorption in the visible spectrum, a high electron injection rate, high turnover rates, and high stability in photoelectrochemical cells.[14,16] The basic transitions that occur in such a solar cell are summarized in Scheme 1.

Electrochemical studies of the thermodynamically important $[L_2Ru(NCS)_2]^{0/+}$ oxidation process (see Scheme 1) have been reported[14,17] for the case in which the bipyridine ligand is in its protonated form. However, the carboxylic acid groups of the dcbpy ligand, in addition to facilitating attachment to electrodes, also enable the L_2RuX_2 sensitizers to participate in acid−base reactions, which could significantly alter the electronic properties of the dcbpy ligand. Thus, while deprotonated forms of the sensitizer have been reported[18] to provide improved performance in photoelectrochemical cells by increasing the open circuit potential by 50−100 mV,[18] surprisingly few studies[11] have specifically addressed the effect of deprotonation on the thermodynamic or spectral properties of the sensitizer.

In this study we have explored the use of electrochemical reduction of the fully protonated *cis*-L_2RuX_2 ($X = NCS^-, CN^-$) complexes in dimethylformamide (and generation of hydrogen gas) as a means of systematically achieving deprotonation of the photovoltaic sensitizer. Spectroscopic (UV/vis) and voltammetric studies on the reduction and oxidation of the electrochemically generated deprotonated species enable insights to be gained into changes of molecular orbital energy levels that occur with different levels of protonation. The new experimental results, combined with theoretical data provided by molecular orbital calculations, enhance the detailed understanding of the role of the protonation state in the performance of sensitizers used in photoelectrochemical cells.

2. Experimental Section

2.1. Instrumentation, Methods, Reagents, and Compounds. Details concerning the instrumentation, methods, reagents, and compounds used are available in the Supporting Information. The complexes L_2RuX_2 have a cis configuration, as determined by NMR experiments. For convenience, the cis notation will be omitted in the remainder of the paper. All potentials are quoted versus the potential of the Fc^+/Fc couple, obtained from the oxidation of ferrocene (Fc) under the same experimental conditions (method, solvent, electrolyte, and temperature) as those used in the relevant experiment. In-house-constructed platinum and glassy carbon macro- and microdisk electrodes of stated diameter were used in all voltammetric experiments, while bulk electrolysis was carried out at a platinum gauze or cylindrical single-piece glassy carbon working electrode. HPLC grade dimethylformamide (DMF), with less than 0.005% water content, was used as the solvent. The electrolyte used for voltammetric experiments was tetrabutylammonium hexafluorophosphate (Bu_4NPF_6). The MOPAC-97 software package (Fujitsu Ltd., Tokyo, Japan) was used for molecular orbital calculations. All calculations employed the semiempirical MNDO-PM3 Hamiltonian.

2.2. Synthesis of Tetrabutylammonium "Salts". Tetrabutylammonium "salts" of the sensitizers[11,18] used for reference against deprotonated solutions prepared by electrochemical reduction of L_2RuX_2 were synthesized via two different routes.[11] In the first, solid precipitated after acidification of aqueous $Bu_4N(OH)$ solutions of L_2RuX_2. The "salts" formed via this procedure were separated from the solution by centrifugation and then freeze-dried. This method produced salts of composition $[(H_{2-x/2}\text{-dcbpy}^{x/2-})_2RuX_2](Bu_4N)_x$, where $0.80 \le x \le 1.85$ (x was determined by NMR spectroscopy). A second synthetic approach was utilized to prepare salts with $x \le 2$. In this method, solid L_2RuX_2 was directly mixed with the required amount of aqueous $Bu_4N(OH)$ solution and then freeze-dried under high vacuum to remove excess water. L_2RuX_2 itself contains 2−4 waters of crystallization,[14] and hence some water was always present in the parent compound as well as in the deprotonated salts.

3. Results and Discussion

3.1. Electrochemical Reduction of $L_2Ru(NCS)_2$. (a) Voltammetry in DMF: The Initial Two One-Electron Reduction Processes. To establish a reference point against which to measure changes induced by deprotonation, detailed knowledge of the voltammetric behavior of $L_2Ru(NCS)_2$ is required. The reduction of $[Ru(bpy)_3]^{2+}$ (bpy = 2,2′-bipyridine) and related compounds usually occurs via an extensive series of reversible one-electron ligand-based charge-transfer processes.[1,19] For example, the ester analogue[20] of $L_2Ru(NCS)_2$ exhibits two chemically and electrochemically reversible reduction processes in DMF with half-wave potentials ($E^r_{1/2}$) of −1.48 and −1.70 V vs Fc/Fc^+ at room temperature at glassy carbon and platinum electrodes, which may be extended to four reversible processes at $T = -58$ °C ($E^r_{1/2} = -1.49$, −1.67, −2.16, and −2.43 V). Since the electronic effect on the pyridine ring arising from esterfication is expected to be negligible, it would be expected that fully protonated $L_2Ru(NCS)_2$ should show analogous voltammetric reduction behavior.

The cyclic voltammetric response observed at a glassy carbon electrode (Figure 1a) in DMF over the potential range from −0.5 to −1.9 V vs Fc/Fc^+ consists of two well-defined processes, the first being chemically reversible, as expected (Figure 1b), and the second, while only partially reversible in the chemical sense, still occurs in the expected potential region. If these initial two reduction processes are H_2-dcbpy ligand based, as is known to be the case with the ester analogue, the initial charge-transfer processes may be formulated as in

(12) Grätzel, M. *Chem. Ing. Technol.* **1995**, *67*, 1300−1305.
(13) O'Regan, B.; Grätzel, M. *Nature (London)* **1991**, *353*, 737−740.
(14) (a) Nazeeruddin, M. K.; Kay, A.; Rodicio, I.; Humphry-Baker, R.; Muller, E.; Liska, P.; Vlachopoulos, N.; Grätzel, M. *J. Am. Chem. Soc.* **1993**, *115*, 6382−6390. (b) Kohle, O.; Ruile, S.; Grätzel, M. *Inorg. Chem.* **1996**, *35*, 4779−4787.
(15) Hagfeldt, A.; Didriksson, B.; Palmqvist, T.; Lindstrom, H.; Sodergren, S.; Rensmo, H.; Lindquist, S. E. *Sol. Energy Mater. Sol. Cells* **1994**, *31*, 481−488.
(16) Kohle, O.; Grätzel, M.; Meyer, A. F.; Meyer, T. B. *Adv. Mater.* **1997**, *9*, 904.
(17) Bond, A. M.; Deacon, G. B.; Howitt, J.; MacFarlane, D. R.; Spiccia, L.; Wolfbauer, G. *J. Electrochem. Soc.* **1999**, *146*, 648−656.
(18) Solaronix Inc., Aubonne, Switzerland, 18 Sept 1999 (http://www.solaronix.ch/products/ruthenium535tba.html).
(19) Elliott, C. M.; Hershenhart, E. J. *J. Am. Chem. Soc.* **1982**, *104*, 7519−7526.
(20) Wolfbauer, G.; Bond, A. M.; MacFarlane, D. R. *J. Chem. Soc., Dalton Trans.* **1999**, in press.

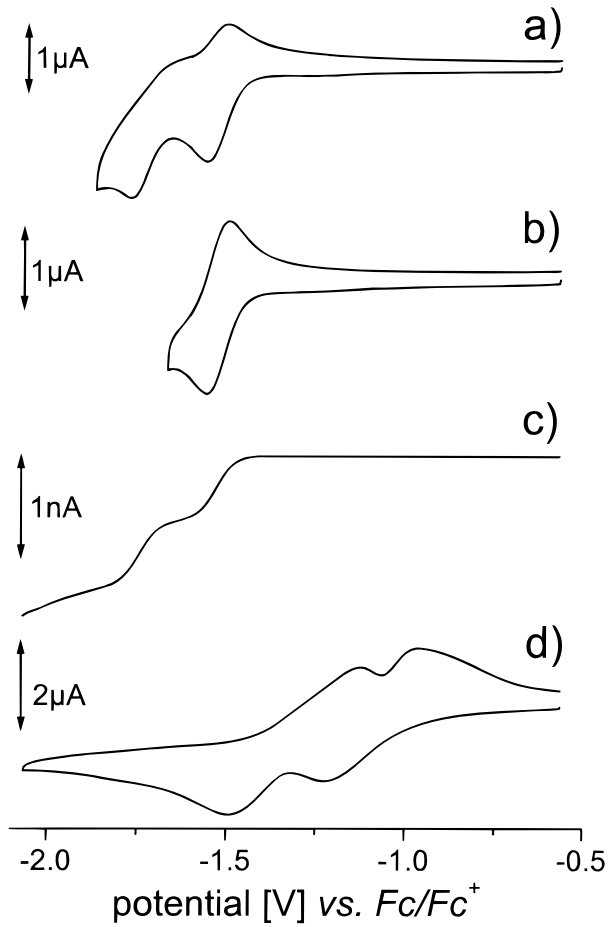

Figure 1. Voltammograms for the first and second $(H_2\text{-dcbpy})_2Ru(NCS)_2$ reduction process at $T = 25$ °C in DMF (0.2M Bu_4NPF_6). (a and b) Cyclic voltammetry ($\upsilon = 100$ mV s^{-1}) at a glassy carbon disk electrode ($d = 1$ mm). (c) Steady-state response ($\upsilon = 20$ mV s^{-1}) at a glassy carbon microdisk electrode ($d = 11.2$ μm). (d) Cyclic voltammetry ($\upsilon = 100$ mV s^{-1}) at a platinum disk electrode ($d = 1$ mm).

eqs 1 and 2 below:

$$(H_2\text{-dcbpy})_2Ru(NCS)_2 + e^- \leftrightharpoons [(H_2\text{-dcbpy}^{\bullet-})(H_2\text{-dcbpy})Ru(NCS)_2]^- \quad (1)$$

$$[(H_2\text{-dcbpy}^{\bullet-})(H_2\text{-dcbpy})Ru(NCS)_2]^- + e^- \leftrightharpoons [(H_2\text{-dcbpy}^{\bullet-})_2Ru(NCS)_2]^{2-} \quad (2)$$

where H_2-dcbpy$^{\bullet-}$ stands for the singly reduced, fully protonated H_2-dcbpy ligand. Further complex reduction processes at more negative potentials are present at glassy carbon electrodes (see later). Evidence indicating that the first process (eq 1) is reversible in both the chemical and electrochemical senses in DMF (0.2 M Bu_4NPF_6) at a glassy carbon electrode is the fact that the peak-to-peak separation (ΔE_p) for the reduction (E_p^{red}) and oxidation (E_p^{ox}) peak potentials was 65 ± mV over the scan rate range of 20−500 mV s^{-1} (concentration $c_0 = 1.1$ mM, temperature $T = 25$ °C), which is close to the theoretically predicted value of 57 mV for a reversible one-electron process. Values of ΔE_p as a function of scan rate are contained in Table 1. At the glassy carbon electrode, the peak−current ratio, i_p^{red}/i_p^{ox} (i_p^{ox} = oxidation peak current, i_p^{red} = reduction peak current), also was close to the theoretically expected value of 1.0 over the scan rate range of 20−5000 mV s^{-1} (see Table 1). Furthermore, the reversible half-wave potential or $E_{1/2}^r$ value (see Table 1) calculated from the values of $(E_p^{ox} + E_p^{red})/2$ (cyclic voltammetry) and the potential at $i_L/2$ (rotating disk electrode, where i_L is the limiting current) is independent of scan rate and rotation rate, respectively, as required for a reversible process. The measured value of $E_{1/2}^r = -1525 \pm 3$ mV is similar to $E_{1/2}^r = -1480$ mV found for the ethyl ester derivative.[20] A plot of i_p^{ox} versus $\upsilon^{1/2}$ from cyclic voltammograms (υ = scan rate) is linear over the scan rate range from 10 to 5000 mV s^{-1}, confirming that the process is diffusion controlled. Mass transport control (diffusion and convection) also was demonstrated via the linear dependence of i_L on $\omega^{1/2}$ ($\omega = 2\pi f$ = angular velocity) in rotating disk electrode experiments.

A voltammogram for the initial process obtained under near-steady-state conditions at a glassy carbon microdisk electrode (Figure 1c) was well defined, and the calculated $E_{1/2}^r$ value coincided with that obtained from cyclic and rotated electrode techniques (see Table 1). The essentially ideal reversible one-electron process observed at a glassy carbon microdisk electrode, compared to minor deviations encountered in other techniques under some conditions (cyclic voltammetry at high scan rates and rotating disk electrode at high rotation rates), suggests that a small amount of uncompensated resistance is present when techniques based on the use of macrodisk electrodes are used.

Confirmation of an initial one-electron charge-transfer process was obtained by noting that plots of E versus $\log((i_L - i)/i)$ ("log-plot", with E = potential and i = current) were linear and had values close to $2.30RT/F$ (59 mV at 25 °C) at rotating macrodisk and microdisk glassy carbon electrodes (see Table 1). Data obtained from rotated disk electrode measurements and use of the Levich equation,[21]

$$i_L = 0.620\,F\,A\,D^{2/3}\,\omega^{1/2}\,\nu^{-1/6}\,c_0 \quad (3)$$

where F is Faraday's constant, c_0 is the bulk concentration, ν is the kinematic viscosity of the solvent, and D is the diffusion coefficient, enabled a value of $D = (2.8 \pm 0.2) \times 10^{-6}$ cm^2 s^{-1} to be calculated for the protonated form of the $L_2Ru(NCS)_2$ complex in DMF.

The observation of chemical reversibility of the second reduction process (eq 2) at a glassy carbon electrode requires the use of cyclic voltammetric scan rates greater than 5000 mV s^{-1} where the i_p^{red}/i_p^{ox} ratio for this process approached unity (see Table 1). Under near steady-state conditions with glassy carbon microdisk and rotating disk electrodes (rotation rates >1000 rpm), the second process showed reversible behavior. $E_{1/2}^r$ values obtained from the latter two techniques coincided with $(E_p^{ox} + E_p^{red})/2$ values obtained from cyclic voltammograms at scan rates $\upsilon > 1500$ mV s^{-1}. "Log-plot" analysis of the second process gave slopes close to the theoretical value expected for a reversible one-electron process. At −58 °C and at glassy carbon electrodes, the initial two $L_2Ru(NCS)_2$ reduction processes are both chemically and electrochemically reversible even under longer time scale conditions (Figures 2a and b). Thus, under conditions of cyclic voltammetry, i_p^{red} for both processes scaled linearly with $\upsilon^{1/2}$ and i_p^{red}/i_p^{ox} values are close to unity over the entire scan rate range (20 to 5000 mV s^{-1}). Furthermore, "log-plots" from rotated disk electrode voltammograms recorded at this temperature gave slopes of 48 ± 6 mV for both processes, which are close to the theoretical expected value of 43 mV at this temperature. The Levich plot (rotated disk electrode) was linear and passed through the origin for both processes. $E_{1/2}^r$ values and other data obtained from glassy carbon electrode voltammograms at −58 °C are reported in Table 2 for both processes.

Even casual inspection of a cyclic voltammogram obtained for reduction of $L_2Ru(NCS)_2$ in DMF (0.1 M Bu_4NPF_6) at a 1

(21) Bard, A. J.; Faulkner, L. R. *Electrochemical Methods*; John Wiley & Sons Inc.: New York, 1980; Chapter 8.3, pp 283−298.

Table 1. Voltammetric Data Obtained for the Reduction (T = 25 °C) of 1.1 mM $(H_2\text{-dcbpy})_2Ru(NCS)_2$ in DMF (0.2 M Bu_4NPF_6) and Oxidation of Deprotonated $[(H_{2-x/2}\text{-dcbpy}^{x/2-})_2Ru(NCS)_2]^{x-}$ at Glassy Carbon Electrodes as a Function of Scan Rate and Rotation[a]

Cyclic Voltammetry[b]						Rotating Disk Electrode[c]		
$[(H_2\text{-dcbpy})_2Ru(NCS)_2]^{0/-}$								
υ / mVs^{-1}	E_p^{red} / mV	E_p^{ox} / mV	ΔE_p / mV	$E^r_{1/2}$ / mV	$\lvert i_p^{red}/i_p^{ox}\rvert$	f / min^{-1}	slope / mV	$E^r_{1/2}$ / mV
10	−1560	−1489	71	−1525	1.34	500	66	−1522
26	−1557	−1497	60	−1527	1.08	1000	67	−1525
50	−1555	−1493	62	−1524	1.07	1500	65	−1527
100	−1555	−1493	62	−1524	1.08	2000	64	−1527
200	−1557	−1491	66	−1524	1.10	2500	62	−1530
500	−1559	−1489	70	−1524	1.08	3000	64	−1529
1000	−1565	−1487	78	−1526	1.04	Microdisk Electrode		
2000	−1577	−1479	98	−1528	1.08	d / μm	slope / mV	$E^r_{1/2}$ / mV
5000	−1601	−1453	145	−1527	1.07	11.2	59	−1525
$[(H_2\text{-dcbpy})_2Ru(NCS)_2]^{-/2-}$								
υ / mVs^{-1}	E_p^{red} / mV	E_p^{ox} / mV	ΔE_p / mV	$E^r_{1/2}$ / mV	$\lvert i_p^{red}/i_p^{ox}\rvert$	f / min^{-1}	slope / mV	$E^r_{1/2}$ / mV
1000	−1785	–	–	–	–	500	–	–
1500	−1791	−1665	−126	−1728	1.45	1000	66	−1747
2000	−1795	−1679	−116	−1737	1.26	1500	66	−1751
3000	−1801	−1683	−118	−1742	1.19	2000	66	−1752
4000	−1809	−1675	−134	−1742	1.12	2500	65	−1753
5000	−1817	−1667	−150	−1742	1.09	3000	64	−1754
						Microdisk Electrode		
						d / μm	slope / mV	$E^r_{1/2}$ / mV
						11.2	57	−1742
$[(H_{2-x/2}\text{-dcbpy}^{x/2-})_2Ru(NCS)_2]^{x-/(x-1)-}$								
υ / mVs^{-1}	E_p^{ox} / mV	E_p^{red} / mV	ΔE_p / mV	$E^r_{1/2}$ / mV	$\lvert i_p^{red}/i_p^{ox}\rvert$	f / min^{-1}	slope / mV	$E^r_{1/2}$ / mV
20	130	40	90	87	–	500	85	83
50	126	56	70	93	2.40	1000	84	88
100	126	56	70	93	1.60	1500	83	89
200	134	52	82	95	1.44	2000	88	92
500	138	52	86	95	1.55	2500	91	93
1000	140	48	92	96	1.54	3000	89	92
2000	154	34	120	96	1.42	3000	89	92

[a] Peak potentials are reported versus Fc/Fc^+ with an uncertainty of ±2 mV. Cyclic voltammetric $E^r_{1/2}$ values calculated as $(E_p^{ox} + E_p^{red})/2$, for steady-state techniques slopes and $E^r_{1/2}$ calculated from "log-plots" (υ = scan rate, f = rotation frequency, d = electrode diameter, E_p = peak potential, $\Delta E_p = E_p^{ox} - E_p^{red}$, i_p = peak current). [b] Glassy carbon electrode d = 1 mm. [c] Glassy carbon electrode d = 3 mm.

Table 2. Summary of Electronic Spectral Data and Reversible Half-Wave Potentials for $(H_2\text{-dcbpy})_2RuX_2$ and the Deprotonated Form $([(H_{2-x/2}\text{-dcbpy}^{x/2-})_2RuX_2]^{x-})$

	electrochemical data,[a] $E^r_{1/2}$ [mV]			spectroscopic data,[b] energy [10^3 cm^{-1}] (molar extinction [10^3 M^{-1} cm^{-1}])		
complex	$Ru^{II/III}$ oxidation	L/L^- reduction	L^-/L^{2-} reduction	$L\pi \rightarrow L\pi^*$	MLCT $Md_\pi \rightarrow L\pi_2^*$	MLCT $Md_\pi \rightarrow L\pi_1^*$
$(H_2\text{-dcbpy})_2Ru(NCS)_2$	+390 ± 10[c]	−1525 ± 4 −1549 ± 3[d]	−1742 ± 5 −1724 ± 4[d]	31.5 (51.6)	24.8 (15.1)	18.3 (15.3)
$[(H_{2-x/2}\text{-dcbpy}^{x/2-})_2Ru(NCS)_2]^{x-}$	+93 ± 5	−2154 ± 5	−2500 ± 10	32.5 (45.7)	26.7 (14.7)	19.4 (14.1)
$(H_2\text{-dcbpy})_2Ru(CN)_2$	+568 ± 5	−1624 ± 10 −1634 ± 5[d]	−1808 ± 10[d]	31.7 (46.8)	25.2 (14.3)	18.7 (17.1)
$[(H_{2-x/2}\text{-dcbpy}^{x/2-})_2Ru(CN)_2]^{x-}$	+210 ± 5	−2267 ± 5	−2617 ± 8	32.7 (42.4)	27.5 (13.1)	19.7 (14.9)

[a] Electrochemical data are obtained from voltammetry at glassy carbon electrodes, and potentials are referenced against Fc/Fc^+. [b] Data obtained by in situ electrolysis in an OTTLE (platinum gauze) experiment. [c] Value taken from ref 17. [d] T = −58 °C; other data obtained at 25 °C.

mm diameter platinum disk electrode (Figure 1d) shows that great differences are found relative to that at glassy carbon. This platinum electrode dependence differs from the voltammetric behavior reported for the ester analogue[20] and $[Ru(bpy)_3]^{2+}$,[1,17] where results are independent of electrode material. Thus, at the platinum surface, the initial reduction processes for $L_2Ru(NCS)_2$ are both very drawn out relative to the response expected for a reversible process, and even more significantly the peak potential of the first process (E_p^{red} = −1.20V vs Fc/Fc^+) is about 0.3 V less negative than predicted on the basis of data obtained with the ester analogue. Even at −58 °C, cyclic voltammograms obtained at a platinum electrode for the reduction of $L_2Ru(NCS)_2$ remain irreversible and highly complex (Figure 2c), although the reduction peak potentials are now in the same region as those at glassy carbon electrodes.

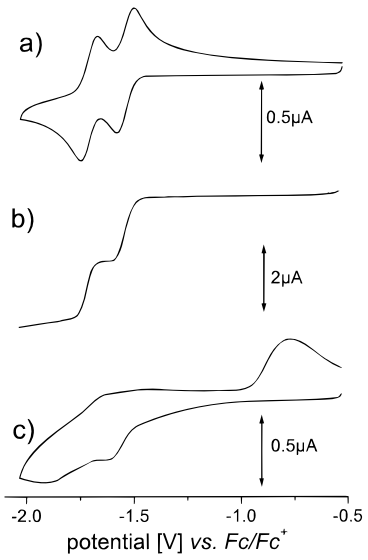

Figure 2. Voltammograms for the first two $(H_2\text{-dcbpy})_2Ru(NCS)_2$ reduction processes at $T = -58$ °C in DMF (0.1 M Bu_4NPF_6). (a) Cyclic voltammetry ($v = 100$ mV s^{-1}) at a glassy carbon disk electrode ($d = 1$ mm). (b) Steady-state voltammogram at a glassy carbon rotating disk electrode ($f = 500$ rpm, $d = 3$ mm). (c) Cyclic voltammetry ($v = 100$ mV s^{-1}) at a platinum disk electrode ($d = 1$ mm).

Thus, in summary, the voltammetry of $L_2Ru(NCS)_2$ at platinum electrodes contains unexpected but, as it will emerge, very useful characteristics that provide voltammetry that is distinctly different from that at glassy carbon, where the first two processes exhibit essentially the behavior expected for this class of compound.

(b) Bulk Reductive Electrolysis at Platinum Electrodes in DMF. The origin of the complex voltammograms at the platinum electrode was probed first of all by exhaustive bulk electrolysis experiments under controlled potential conditions at a large area platinum gauze working electrode at 25 °C. In initial experiments, the potential was set to −2.0 V vs Fc/Fc^+ (more negative than the second $L_2Ru(NCS)_2$ reduction process detected at glassy carbon and platinum electrodes) and the electrolysis of 0.5−2.0 mM solutions allowed to go to completion (30−40 min). Coulometric analysis under these conditions revealed that 3.35 ± 0.35 electrons per molecule were involved in the complete reaction. Gas chromatographic measurements of the collected gas phase showed molecular hydrogen as being the significant gaseous product. The peak intensity of the hydrogen signal was close to that expected if the majority of electrons transferred were used for the formation of hydrogen. On the basis of the coulometry and hydrogen data, the overall reaction observed at platinum electrodes on the time scale of bulk electrolysis at −2.0 V vs Fc/Fc^+ at a platinum electrode can be said, for initial discussion purposes, to correspond approximately to an overall deprotonation reaction of the kind

$$(H_2\text{-dcbpy})_2Ru(NCS)_2 + 4e^- \rightarrow [(dcbpy^{2-})_2Ru(NCS)_2]^{4-} + 2H_2 \quad (4)$$

For the sake of clarity, $dcbpy^{2-}$ and $H\text{-dcbpy}^-$ will be used throughout the remainder of this paper for the doubly and singly deprotonated H_2-dcbpy ligand, respectively. In contrast, $H_2\text{-dcbpy}^{\bullet-}$ will be used for the singly reduced but fully protonated H_2-dcbpy ligand. Mixed forms of the ligand (deprotonated and reduced) will be abbreviated accordingly. The overall charge of the complexes is given outside the square brackets.

Clearly, an extensive sequence of electron-transfer and chemical reactions can occur at the platinum surface which involves steps where H^+ is formed by deprotonation before or after an electron-transfer reaction and H_2 is generated heterogeneously at the electrode surface or homogeneously by solution-phase reactions. One example of heterogeneous generation of H_2 that gives the overall reaction in eq 4 would be the reaction sequence in eqs 5−7:

$$(H_2\text{-dcbpy})_2Ru(NCS)_2 \leftrightharpoons [(H\text{-dcbpy}^-)_2Ru(NCS)_2]^{2-} + 2H^+ \quad (5)$$

$$[(H\text{-dcbpy}^-)_2Ru(NCS)_2]^{2-} \leftrightharpoons [(dcbpy^{2-})_2Ru(NCS)_2]^{4-} + 2H^+ \quad (6)$$

$$4H^+ + 4e^- \rightarrow 2H_2 \quad (7)$$

Or, if hydrogen is generated by homogeneous reactions after electron transfer, then eqs 8−10 would represent one of many possible series of reaction pathways that give the overall eq 4:

$$(H_2\text{-dcbpy})_2Ru(NCS)_2 \leftrightharpoons [(dcbpy^{2-})_2Ru(NCS)_2]^{4-} + 4H^+ \quad (8)$$

$$2(H_2\text{-dcbpy})_2Ru(NCS)_2 + 4e^- \leftrightharpoons 2[(H_2\text{-dcbpy}^{\bullet-})_2Ru(NCS)_2]^{2-} \quad (9)$$

$$2[(H_2\text{-dcbpy}^{\bullet-})_2Ru(NCS)_2]^{2-} + 4H^+ \rightarrow 2(H_2\text{-dcbpy})_2Ru(NCS)_2 + 2H_2 \quad (10)$$

These sequences of reactions are possible because the protonated $(H_2\text{-dcbpy})_2Ru(NCS)_2$ sensitizer may exist in an acid−base equilibrium (eqs 5 and 8), the extent to which deprotonation occurs being dependent on solvent (medium)-specific pK_a values. Thus, it needs to be noted that, in the presence of water, adventitiously present or deliberately added, thermodynamic (and/or kinetic) limitations will be placed on the extent to which reduction can occur via the acid equilibrium dissociation because of the following reaction:

$$[(dcbpy^{2-})_2Ru(NCS)_2]^{4-} + y\,H_2O \leftrightharpoons [(H_{y/2}\text{-dcbpy}^{(2-y/2)-})_2Ru(NCS)_2]^{(4-y)-} + y\,OH^- \quad (11)$$

Thermodynamically, protons can very easily be reduced to hydrogen, although the suppression of the heterogeneous reaction pathway can be achieved by choice of an appropriate electrode material, at which the rate of this reaction is electrochemically negligible at the reversible potential.[22] Glassy carbon is an electrode material in which the overpotential for the reduction of protons to hydrogen is very large. In contrast, the overpotential for the generation of hydrogen at platinum electrodes is small. Reduced ruthenium polypyridine compounds are known to catalytically reduce protons or residual water to hydrogen in organic solvents.[23] Thus, the reaction sequence described in eqs 9 and 10 might be a source of hydrogen generation, at least under long time scale conditions. However, the hydrogen producing step in eq 10 is based on a purely homogeneous solution-phase reaction and does not predict the experimentally observed influence of electrode material. In contrast, the electrochemical reduction of protons (eq 7), made available by the acid−base equilibrium described in eqs 5, 6, and 8, and occurs at the electrode surface, and hence heterogeneous electrode kinetics may be involved in the reaction sequence, which could explain the electrode material-dependent voltammetric responses observed for the reduction of $(H_2\text{-dcbpy})_2Ru(NCS)_2$.

Overall, eq 4 predicts the transfer of 4.0 electrons per molecule if complete deprotonation occurs to quantitatively yield $[(dcbpy^{2-})_2Ru(NCS)_2]^{4-}$, whereas the measured number of electrons transferred was only 3.35 ± 0.35. Hence, this equation

(22) Bard, A. J.; Faulkner, L. R. *Electrochemical Methods*; John Wiley & Sons Inc.: New York, 1980.

(23) Abruña, H. D.; Teng, A. Y.; Samuels, G. J.; Meyer, T. J. *J. Am. Chem. Soc.* **1979**, *101*, 6745−6746.

and the mechanism given as examples cannot provide a complete description of the process. The pK_a values of $(H_2\text{-dcbpy})_2Ru(NCS)_2$ in DMF are unknown, although $(H_2\text{-dcbpy})_2Ru(NCS)_2$ would be expected to be a weak acid, since conductivity measurements have shown[17] that the complex is present predominantly in its protonated form in most organic solvents. However, the first two pK_a values for the $(H_2\text{-dcbpy})_2Ru(NCS)_2$ complex are expected to be relatively low in comparison to those reported[24] for $[Ru(H_2\text{-dcbpy})_2(bpy)]^{2+}$ in water, so that at least two protons are likely to be relatively easy to remove.

Finally, it needs to be noted that, since residual water is present, the reaction sequence

$$(H_2\text{-dcbpy})_2Ru(NCS)_2 + 2\,e^- \rightarrow [(H_2\text{-dcbpy}^{\bullet-})_2Ru(NCS)_2]^{2-} \quad (12)$$

$$[(H_2\text{-dcbpy}^{\bullet-})_2Ru(NCS)_2]^{2-} + 2\,H_2O \leftrightharpoons (H_2\text{-dcbpy})_2Ru(NCS)_2 + 2\,OH^- + H_2 \quad (13)$$

$$(H_2\text{-dcbpy})_2Ru(NCS)_2 + 2\,OH^- \leftrightharpoons [(H\text{-dcbpy}^-)_2Ru(NCS)_2]^{2-} + H_2O \quad (14)$$

would give the overall reaction

$$(H_2\text{-dcbpy})_2Ru(NCS)_2 + 2\,H_2O + 4\,e^- \leftrightharpoons [(H\text{-dcbpy}^-)_2Ru(NCS)_2]^{2-} + 2\,OH^- + 2\,H_2 \quad (15)$$

In summary, this reaction with water can be generally written as

$$(H_2\text{-dcbpy})_2Ru(NCS)_2 + (z\text{-}2)H_2O + ze^- \rightarrow [(H\text{-dcbpy}^-)_2Ru(NCS)_2]^{2-} + (z-2)OH^- + \tfrac{z}{2}H_2 \quad (16)$$

This reaction sequence also is consistent with our data (vide infra). Clearly, a range of combinations of electron- and proton-transfer steps are possible (see above) which lead to deprotonation. However, the reaction scheme can be very complex, and formation of equilibrium quantities of singly and triply deprotonated $L_2Ru(NCS)_2$ complexes also can occur, as can a potential-dependent combination of reaction pathways. Thus, the 3.35 ± 0.35 electrons transferred in bulk electrolysis at -2.0 V reflects the overall extent of a complex sequence of reactions at this potential that form $[(H_{2-x/2}\text{-dcbpy}^{x/2-})_2Ru(NCS)_2]^{x-}$, where x is the number of protons removed.

To probe the identity of the deprotonated species produced during electrolysis, a 1.1 mM solution of $L_2Ru(NCS)_2$ again was reduced in DMF at a platinum gauze electrode using the same conditions as before. However, on this occasion, the course of the reaction was monitored (Figure 3) by cyclic voltammetry at a glassy carbon electrode over a more negative potential regime, where the existence of an extended series of processes is revealed (Figure 3a). When voltammetric monitoring is undertaken over this wider potential range (Figure 3a−e), the initial two processes identified above, as well as the other processes in the more negative potential region, ultimately are replaced by two new, well-defined processes in the very negative potential region (Figure 3e). As may be expected, cyclic voltammograms obtained on partially rather than exhaustively reduced solutions (Figure 3b−d) are complicated. The particular exhaustive bulk electrolysis shown in Figure 3 consumes 3.5 electrons per molecule and leads to detection of one chemically and electrochemically reversible process, followed by a partially reversible process at the glassy carbon electrode. However, despite the complexity of the initial steps of electrolysis, the final form of the glassy carbon cyclic voltammogram detected from solutions exhaustively reduced at platinum electrodes at -2.0 V simply consists of two processes with $E^r_{1/2}$ values that

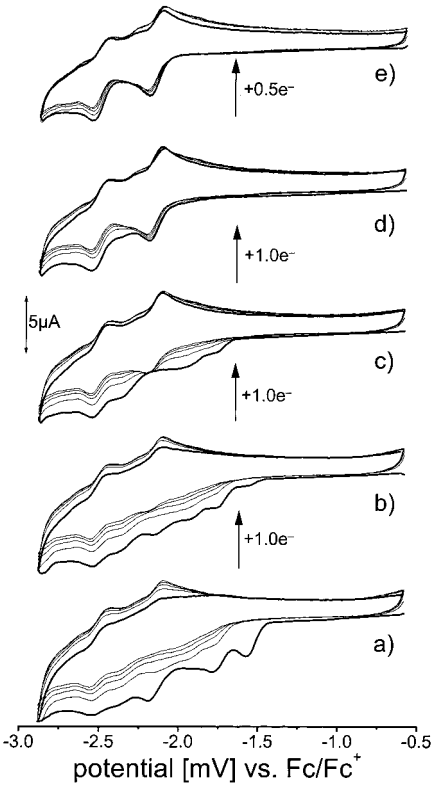

Figure 3. Cyclic voltammograms ($v = 1000$ mV s^{-1}, initial five scans, first scan bold) obtained at a glassy carbon working electrode ($d = 1$ mm) for reduction of 1.1 mM $(H_2\text{-dcbpy})_2Ru(NCS)_2$ in DMF (0.1 M Bu_4NPF_6) at different stages of reductive bulk electrolysis ($E_{appl} = -2.05$ V) at a platinum gauze electrode. (a) Before electrolysis commences, (b) one electron transferred, (c) two electrons transferred, (d) three electrons transferred, and (e) 3.5 electrons transferred (exhaustive electrolysis).

are about 0.65 V more negative than the initial two processes for reduction of $(H_2\text{-dcbpy})_2Ru(NCS)_2$.

Detailed analysis of voltammograms at glassy carbon electrodes of the two reduction processes observed after exhaustive electrolysis at $E_{appl} = -2.0$ V vs Fc/Fc$^+$ reveals that i_p^{red} for the first process (cyclic voltammetry) scaled linearly with $v^{1/2}$. Furthermore, Levich plots (rotated glassy carbon disk electrode) were linear and passed through the origin for both processes, establishing that they are mass transport controlled. The slope of the Levich plot gave a diffusion coefficient for $[(H_{2-x/2}\text{-dcbpy}^{x/2-})_2Ru(NCS)_2]^{x-}$ (x = number of protons removed) of $D = (2.5 \pm 0.4) \times 10^{-6}$ cm^2 s^{-1}, which is very similar to the value obtained for the fully protonated form. The $E^r_{1/2}$ value for the initial reduction process (cyclic and rotated disk techniques) was calculated to be -2155 ± 5 mV vs Fc/Fc$^+$. "Log-plots" (rotated disk voltammograms) gave slopes of 70 ± 2 mV, which are close to the theoretical value expected for a reversible one-electron process. Scan rates greater than 2000 mV s^{-1} were required in order to make the second reduction process fully reversible. Under steady-state conditions at the rotating disk electrode, the second process also is close to reversible. Thus, $E^r_{1/2}$ values calculated from "log-plots" for the second process (rotated disk) are in agreement with the value of $(E_p^{ox} + E_p^{red})/2$ obtained from cyclic voltammograms ($v > 200$ mV s^{-1}). The reversible half-wave potential for the second reduction process of $[(H_{2-x/2}\text{-dcbpy}^{x/2-})_2Ru(NCS)_2]^{x-}$, therefore, is established to be -2500 ± 10 mV vs Fc/Fc$^+$.

In another series of bulk electrolysis experiments at the platinum gauze electrode, the solution of electrogenerated

(24) Nazeeruddin, M. K.; Kalyanasundaram, K. *Inorg. Chem.* **1989**, *28*, 4251−4259.

$[(H_{2-x/2}\text{-dcbpy}^{x/2-})_2Ru(NCS)_2]^{x-}$ was further reduced at a potential of $E_{appl} = -2.3$ V (i.e., more negative than the reversible potential of the first new reduction process for the deprotonated form of $L_2Ru(NCS)_2$). Monitoring the course of this experiment by glassy carbon rotating disk electrode measurements indicated that conversion of the desired product back to the originally present $[(H_{2-x/2}\text{-dcbpy}^{x/2-})_2Ru(NCS)_2]^{x-}$ form of the ruthenium complex occurred. Moreover, hydrogen was detected by gas chromatographic analysis of the gas phase present above the sample. This reaction pathway would be expected if the $[(H_{2-x/2}\text{-dcbpy}^{x/2-})_2Ru(NCS)_2]^{(x+1)-}$ compound can reduce residual water or even the electrolyte or solvent to regenerate $[(H_{2-x/2}\text{-dcbpy}^{x/2-})_2Ru(NCS)_2]^{x-}$, which is the initial form of the complex and hydrogen gas,[23,25] in a form of reaction similar to that postulated for reaction of reduced forms of $(H_2\text{-dcbpy})_2Ru(NCS)_2$ with water (eq 10). Alternatively, an even less protonated form might be initially generated with evolution of hydrogen but then react with residual water to re-form the more protonated form. Prolonged reduction periods of >20 min at −2.3 V resulted in slow decomposition of $[(H_{2-x/2}\text{-dcbpy}^{x/2-})_2Ru(NCS)_2]^{x-}$, as determined by voltammetric monitoring at glassy carbon electrodes. Thus, a slow decomposition reaction is available for this species as an alternative to the hydrogen evolution redox reactions considered above.

To verify that deprotonation and hydrogen evolution could occur at potentials prior to the reversible potential established at glassy carbon electrodes for the $[(H_2\text{-dcbpy})Ru(NCS)_2]^{0/-}$ process, solutions of $L_2Ru(NCS)_2$ were reductively electrolyzed at platinum electrodes at a potential of −1.2 V vs Fc/Fc^+. This potential in fact corresponds to the foot of the initial reduction wave observed at platinum electrodes (Figure 1d) and therefore is significantly less negative than the reversible potential for the first ligand-based reduction process ($E^r_{1/2} = -1.53$ V, see Table 2). Exhaustive electrolysis at this potential required a longer time span of 90−180 min. Again, hydrogen gas was detected as a product of electrolysis. The number of electrons transferred at this potential was 2.5 ± 0.5, and a cyclic voltammogram obtained after electrolysis was similar to those observed for partial electrolysis at −2.0 V (Figure 3b,c), implying that only partial deprotonation occurred under these conditions. When the electrolysis was allowed to continue at −2.0 V, a further 1.0 ± 0.5 electrons were consumed, so that the sum of both forms of electrolysis gives rise to the transfer of as many electrons as when exhaustive electrolysis was carried out at −2.0 V in a single step. As expected, a cyclic voltammogram at a glassy carbon electrode of the solution electrolyzed in these two stages was identical to that shown in Figure 3e, which indicates that the same deprotonated products are formed during electrolysis at positive potentials. Importantly, this last data set leads to the conclusion that reductive electrolysis and deprotonation of $L_2Ru(NCS)_2$ at platinum electrodes can proceed via the heterogeneous reduction at −1.2 V of protons at a platinum electrode surface, since the thermodynamic requirement for the homogeneous formation of hydrogen via ligand-reduced forms of $L_2Ru(NCS)_2$ (eqs 8−10) is not met at this potential.

(c) Bulk Electrolysis at Glassy Carbon Electrodes. When bulk reductive electrolysis of $L_2Ru(NCS)_2$ was attempted at −1.2 V vs Fc/Fc^+ at a glassy carbon cup electrode, no appreciable reaction could be detected. This result is as expected from cyclic voltammetric data obtained at glassy carbon and also confirms that the heterogeneous reaction pathway for hydrogen production at this electrode material is negligible. However, when the electrolysis was carried out at −2.0 V vs Fc/Fc^+, exhaustive electrolysis proceeded as observed when platinum electrodes were used, although the reaction needed a longer time for completion. Cyclic voltammetric and gas chromatographic monitoring of this reaction, carried out as described above after electrolysis at a platinum basket electrode, showed that the reaction occurred in the same overall manner as that observed at platinum electrodes. That is, deprotonated forms of the $L_2Ru(NCS)_2$ complex and hydrogen gas were formed. In contrast to platinum electrodes, at this electrode material hydrogen formation predominately will have occurred via the homogeneous pathway described in eqs 8−10. It is noted that, after electrolysis, minor decomposition products were detectable by cyclic voltammetry on glassy carbon electrodes, suggesting that additional side reaction pathways are available for the ligand-based reduced forms of $L_2Ru(NCS)_2$.

(d) Molecular Orbital Calculations. The −0.65 V shift in potential of $E^r_{1/2}$ for the ligand-based reduction processes of $(H_2\text{-dcbpy})_2Ru(NCS)_2$ after deprotonation may be attributed to the electronic influence of the carboxylate group on the bpy ligand. In ruthenium polypyridine complexes, the first set of reduction processes are ligand based and are directly related to the energy of the first unoccupied orbital (LUMO or π_1^*) of the polypyridine ligand.[8,26] Due to its −M (M = mesomeric effect) effect, the protonated carboxylate ligand (−COOH) withdraws electron density from the bpy ring, and hence the energy of the LUMO is significantly lowered by about 0.5 eV according to MNDO calculations (see below and ref 26). On the basis of this electronic effect, $(R_2\text{-dcbpy})_2RuX_2$ (R = C_2H_5 in ref 20 and R = H in this study) should both be easier to reduce than $(bpy)_2RuX_2$,[8] as is confirmed when data available in the literature are examined. Thus, $E^r_{1/2}$ for the first ligand-based reduction process of $(bpy)_2RuX_2$ (X = halogen or pseudohalogen) compounds lies in the range from −1.95 to −2.1 V vs Fc/Fc^+, whereas the initial reduction process $(R_2\text{-dcbpy})_2RuX_2$ occurs between −1.48 and −1.62 V vs Fc/Fc^+. However, if the −COOH group is deprotonated, to give $-COO^-$, the influence of the electronic effect on redox potentials would be expected to be reversed. That is, a significant increase in LUMO energy is expected to occur upon deprotonation, which in turn would be consistent with the observed shift of the reduction processes to more negative potentials.

In an endeavor to quantify the effect of deprotonation of the H_2-dcbpy ligand, semiempirical molecular orbital (MO) calculations were undertaken on the free H_2-dcbpy ligand, its deprotonated forms, and the bpy ligand. The MO approach has been employed[26] to explain the comparative features of electrochemistry of $[Ru(Et_2\text{-dcbpy})_3]^{2+}$ and $[Ru(bpy)_3]^{2+}$, where Et_2-dcbpy is the diethyl ester of H_2-dcbpy. Importantly, we note that the authors of this particular study[26] could predict the potential of the first ligand-based reduction of $[Ru(Et_2\text{-dcbpy})_3]^{2+}$ by comparing the LUMO energies for the free bpy and H_2-dcbpy ligands (H_2-dcbpy was used in these calculations as a model ligand for Et_2-dcbpy).

Prior to undertaking the MO calculations, the ligands of interest were subjected to energy minimization calculations. All bipyridine ligands exhibited an absolute energy minimum with the pyridine nitrogens in a trans position relative to each other. However, to maintain a configuration which is more closely related to the manner in which the bipyridine ligands are known[27,28] to be coordinated to the ruthenium center (see insert in Scheme 1), the ring systems were minimized into a local energy minimum, in which the substituents on both pyridine

(25) Launikonis, A.; Lay, P. A.; Mau, A. W. H.; Sargeson, A. M.; Sasse, W. H. F. *Aust. J. Chem.* **1986**, *39*, 1053−1062.

(26) Ohsawa, Y.; Whangbo, M. H.; Hanck, K. W.; DeArmond, M. K. *Inorg. Chem.* **1984**, *23*, 3426−3428.

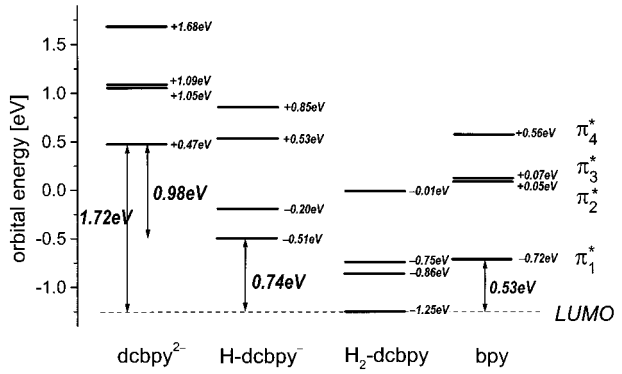

Figure 4. Orbital energy values obtained from MNDO-PM3 calculations.

ring systems are in cis positions relative to each other, although the difference in energy between the trans and cis configurations is very small. In the cis configuration, the pyridine rings are slightly out-of-plane by a tilt angle of $11 \pm 2°$. This nonplanarity of the bipyridine ligands has previously been used to rationalize ESR results obtained from oxidized ruthenium polypyridine complexes.[29] Furthermore, the carboxylic acid groups (−COOH) were out-of-plane with the pyridine ring by $22 \pm 2°$, which is in good agreement with crystallographic data of $(H_2\text{-dcbpy})_2Ru(NCS)_2$, where an angle of 30° has been reported,[28] whereas the carboxylic anion groups ($-COO^-$) were in-plane with the pyridine ring.

The calculated MO data are represented schematically in Figure 4. The π_2*-, π_3*-, and π_4*-orbitals and absolute energy values are included for convenience. The introduction of carboxylic acid groups on the bpy ligand was calculated to lower the π_1*-orbital by 0.53 eV, which is in good agreement with the value of 0.58 eV reported by Ohsawa and co-workers.[26] The drastic effect of deprotonation on the energies of the molecular orbitals and hence the predicted reduction potentials is clearly demonstrated in Figure 4. Removing one proton from H_2-dcbpy increases the energy of the π_1*-orbital by 0.74 eV, which is more than compensated for by the initial 0.53 eV lowering of the electron-withdrawing effect caused by introduction of the carboxylic acid groups. Thus, the π_1* energy of H-dcbpy$^-$ lies beyond that of bpy. The π_1*-orbital of the fully deprotonated ligand, dcbpy^{2-}, lies 1.72 eV higher in energy than that of H_2-dcbpy. Energy density calculations show, that in the case of the partly deprotonated ligand (H-dcbpy$^-$), the π_1*- and π_2*-orbitals are predominantly located on the pyridine moiety containing the protonated acid.

Relative values for the reduction potential of protonated and deprotonated forms of L_2RuX_2 may be estimated from the MO calculations. If $[(\text{H-dcbpy}^-)(\text{H}_2\text{-dcbpy})RuX_2]^-$ is formed, the first reduction process is predicted to be determined by the ligand with the lowest π_1*-orbital, which therefore remains as H_2-dcbpy. In this situation, no dramatic change in the value of the redox potential is expected relative to that for $(H_2\text{-dcbpy})_2Ru(NCS)_2$. In contrast, complete deprotonation, yielding $[(\text{dcbpy}^{2-})_2Ru(NCS)_2]^{4-}$, should result in a negative shift of the potential for the first reduction process by 1.7 V, since the value is now determined by the position of the π_1*-orbital of dcbpy^{2-}. Neither of these scenarios is observed experimentally. However, removal of one proton from each H_2-dcbpy ligand to give the $[(\text{H-dcbpy}^-)_2RuX_2]^{2-}$ complex is predicted to give a reduction potential for the first process which is about 0.7 V more negative than that of $(H_2\text{-dcbpy})_2RuX_2$. The experimental observation of a potential difference of 0.65 V between the protonated and electrochemically deprotonated complex therefore implies that electrochemical reduction of $L_2Ru(NCS)_2$ is likely to have generated the doubly deprotonated anion, $[(\text{H-dcbpy}^-)RuX_2]^{2-}$, rather than singly, triply, or quadruply deprotonated species.

No reports on the reduction of metal-coordinated bipyridine carboxylic acid ligands are available in the literature. However, extensive polarographic studies on acids of single-ring analogues (pyridine derivatives) have been reported in aqueous media.[30−39] For example, the polarographic reduction of isonicotinic and picolinic acids have been studied as a function of pH by Volke and Volková.[31,32] In these reports, changes in the polarographic wave heights and $E^r_{1/2}$ values were discussed in terms of the acid−base behavior of the compounds, although proposed reaction products were not isolated. Lund[30] demonstrated that the reduction of isonicotinic acid at a mercury electrode gives high yields of the corresponding aldehyde in acidic solutions. Campanella and co-workers[37,38] explained the existence of up to five reduction processes for the reduction of dipicolinic and isocinchomeronic acid in terms of acid−base behavior and attributed the origin of some of the processes to a combination of deprotonation, proton reduction, and irreversible formation of molecular hydrogen, although the absence of proof of hydrogen gas formation resulted in criticism of some mechanistic aspects of these studies.[34]

(e) Voltammetry at Positive Potentials as a Function of Deprotonation. On the basis that reduction processes are shifted to more negative potentials by deprotonation, the oxidation should become easier if the metal d-orbitals and ligand orbitals are affected in an analogous manner. Under low scan rate conditions of cyclic voltammetry at macrodisk electrodes, oxidation of $L_2Ru(NCS)_2$ is chemically irreversible and complex in DMF (see Figure 5a and ref 17). The initial process observed in Figure 5a is the metal-based oxidation process, while oxidation behavior at more positive potentials, not considered further in this paper, is related to interaction of $L_2Ru(NCS)_2$ and/or products of electrolysis with the electrode surface.[17] Use of microdisk electrodes and use of very fast scan rates (>100 V s^{-1}) are, in fact, necessary to achieve any evidence of chemical reversibility for the oxidation of protonated $L_2Ru(NCS)_2$.[17]

Despite the irreversibility of some processes and significant interaction with the surface, the influence of deprotonation on the oxidation potential can be determined by periodically recording cyclic voltammograms at a macrodisk glassy carbon electrode over the potential range from −0.6 to +1.0 V during the course of reductive bulk electrolysis at a platinum basket

(27) Shklover, V.; Nazeeruddin, M. K.; Zakeeruddin, S. M.; Barbe, C.; Kay, A.; Haibach, T.; Steurer, W.; Hermann, R.; Nissen, H. U.; Grätzel, M. *Chem. Mater.* **1997**, *9*, 430−439.
(28) Shklover, V.; Ovchinnikov, Y. E.; Braginsky, L. S.; Zakeeruddin, S. M.; Grätzel, M. *Chem. Mater.* **1998**, *10*, 2533 −2541.
(29) Wolfbauer, G.; Bond, A. M.; MacFarlane, D. R. *Inorg. Chem.* **1999**, *38*, 3836−3846.
(30) Lund, H. *Acta Chem. Scand.* **1963**, *17*, 972−978.
(31) Volke, J.; Volková, V. *Collect. Czech. Chem. Commun.* **1955**, *20*, 1332−1339.
(32) Volke, J.; Volková, V. *Collect. Czech. Chem. Commun.* **1955**, *20*, 908−916.
(33) Tissier, C.; Agoutin, M. *J. Electrochem. Soc.* **1973**, *47*, 499−508.
(34) Brown, O. R.; Harrison, J. A.; Sastry, K. S. *J. Electroanal. Chem.* **1975**, *58*, 387−391.
(35) Vlcek, A. A.; Dodsworth, E. S.; Pietro, W. J.; Lever, A. B. P. *Inorg. Chem.* **1995**, *34*, 1906−1913.
(36) Argazzi, R.; Bignozzi, C. A.; Hasselmann, G. M.; Meyer, G. J. *Inorg. Chem.* **1998**, *37*, 4533−4537.
(37) Campanella, L.; Chiacchierini, E.; Palchetti, M. *Rev. Roum. Chim.* **1972**, *17*, 647−660.
(38) Campanella, L.; Cignini, P. L.; de Angelis, G. *Rev. Roum. Chim.* **1973**, *18*, 1649−1657.
(39) Serazetdinova, V. A.; Suvorov, B. V. *Zh. Anal. Khim.* **1978**, *33*, 964−965.

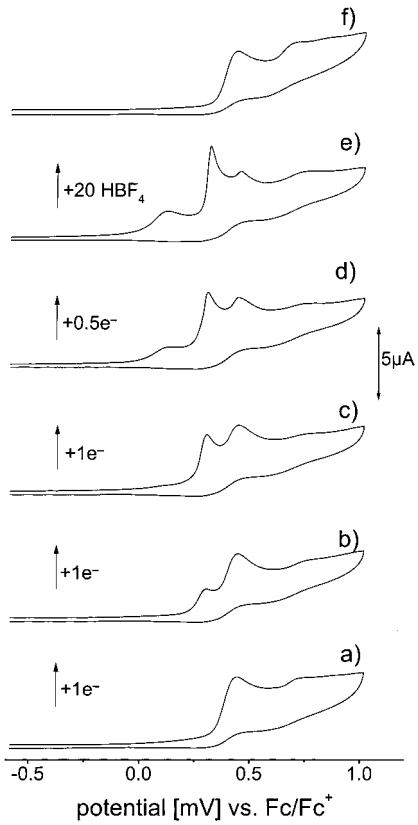

Figure 5. Cyclic voltammograms (v = 100 mV s^{-1}) obtained at a glassy carbon working electrode (d = 1 mm) over the potential range where the metal-based oxidation of 1.1 mM $L_2Ru(NCS)_2$ occurs at a platinum gauze electrode in DMF (0.1 M Bu_4NPF_6) during the course of a reductive bulk electrolysis (E_{appl} = −2030 mV). (a) Before commencement, (b) one electron transferred, (c) two electrons transferred, (d) three electrons transferred, and (e) 3.5 electrons transferred (exhaustive electrolysis). (f) 20 equiv of HBF_4 added to the solution.

mesh electrode (E_{appl} = −2.0 V; experimental details given in the caption to Figure 5). When one electron per $L_2Ru(NCS)_2$ molecule has been transferred, the appearance of a new oxidation process having a peak at a potential about 150 mV less positive than the initial oxidation process maybe noted, as may a decrease in the peak height for the initial process (Figure 5b). This process has the characteristics of surface interaction. As the bulk electrolysis proceeds further (Figure 5c−e) to what is believed to be a deprotonated form of $L_2Ru(NCS)_2$, another new process with different character is detected at an even less positive potential (about 0.3 V prior to oxidation of protonated complex).

After deprotonation by reduction, the first oxidation process is followed by a series of complex processes. As expected, if those new processes are associated with deprotonation and formation of hydroxyl anions, the new processes were also shown to increase in intensity as $Bu_4N(OH)$ is added to solutions of $L_2Ru(NCS)_2$ (also see below). To further support the hypothesis that reduction of $L_2Ru(NCS)_2$ leads to protons being lost by reduction to hydrogen, the exhaustively electrolyzed solution was titrated with an HBF_4 solution in DMF. It was found that the cyclic voltammogram for the oxidation of the fully protonated $(H_2\text{-dcbpy})_2Ru(NCS)_2$ complex could be regenerated by addition of 3.5 ± 0.5 mol equiv of HBF_4 solution to the electrolyzed solution. Thus, within experimental error, the amount of added protons required for regeneration of the protonated complex is equivalent to the number of electrons consumed during the course of reductive electrolysis. On addition of excess acid (≥4 mol equiv), no further changes in the cyclic voltammogram (Figure 5f) are observed, and the

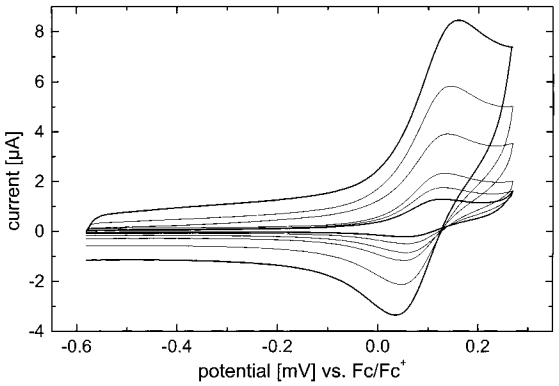

Figure 6. Cyclic voltammograms for the oxidation of electrogenerated $[(H_{2-x/2}\text{-dcbpy}^{x/2-})_2Ru(NCS)_2]^{x-}$ in DMF (0.1 M Bu_4NPF_6) at a glassy carbon electrode as a function of scan rate (v = 50, 100, 200, 500, 1000, and 2000 mV s^{-1}).

voltammogram remains essentially identical to that of the starting solution (Figure 5a). The result obtained from this acid titration experiment is as expected if the postulated mechanism involving formation of deprotonated forms of $L_2Ru(NCS)_2$ via exhaustive electrolysis is correct.

The chemical reversibility of the least positive process detected in exhaustively electrolyzed solutions was assessed under conditions of cyclic voltammetry by switching the potential at about 0.27 V. As shown in Figure 6, the chemical reversibility increases with increasing scan rate. Despite the fact that a peak current ratio (i_p^{ox}/i_p^{red}) of unity is not achieved at scan rates up to 2000 mV s^{-1}, ($E_p^{ox} + E_p^{red}$)/2 values calculated from cyclic voltammograms over the scan rate range of 50−2000 mV s^{-1} were constant within experimental error (see Table 1), as required for a reversible process. Thus, the extent of departure from ideally reversible process must be small, with respect to the influence on peak positions. Under steady-state conditions at a rotating disk electrode ($f \geq$ 2000 min^{-1}), $E_{1/2}^r$ values obtained from "log-plots" were in good agreement with $E_{1/2}^r$ values obtained from cyclic voltammograms. However, the slopes of "log-plots" were slightly larger than theoretically predicted for a reversible process (Table 1). Thus, this initial process detected after exhaustive electrolysis is assigned to the deprotonated $[(H_{2-x/2}\text{-dcbpy}^{x/2-})_2Ru^{II/III}(NCS)_2]^{x-/(x+1)-}$ metal-based oxidation reaction, and the reversible half-wave potential is established to be +93 ± 5 mV. From a Levich plot (rotating disk electrode), the diffusion coefficient for $[(L^{x/2-})_2Ru(NCS)_2]^{x-}$ in DMF is D = (2.7 ± 0.4) × 10^{-6} cm^2 s^{-1}, which is in excellent agreement with the value (D = (2.5 ± 0.4) × 10^{-6} cm^2 s^{-1}) calculated from voltammograms obtained for the reduction processes (see above).

The shift of 0.3 V for oxidation of protonated and deprotonated forms of $L_2Ru(NCS)_2$ reflects the altered electronic environment of the ligands and their influence on the ruthenium metal d-orbitals. The fact that oxidation becomes easier after deprotonation and reduction more difficult is consistent with the increased overall negative charge on the complex that accompanies deprotonation. Interestingly, Zaban and co-workers[40] investigated the oxidation of Ru, Mg, and Fe photovoltaic sensitizer complexes with ligands containing phosphonic or carboxylic acid groups at platinum and glassy carbon electrodes in aqueous media but did not observe a pH dependence. In contrast, a pH dependence attributed to electronic changes in the semiconductor−electrolyte interface was reported when these dyes were attached to semiconductor electrode surfaces.

(40) Zaban, A.; Ferrere, S.; Gregg, B. A. *J. Phys. Chem. B* **1998**, *102*, 452−460.

(f) Studies on Bu_4N Salts of Deprotonated $L_2Ru(NCS)_2$. To relate the significance of the above findings to photovoltaic cells, voltammetric studies on "salts" used in photovoltaic cells[18] were investigated. These "salts" are formed by reaction of $L_2Ru(NCS)_2$ with $Bu_4N(OH)$, which is a very strong base in organic solvents.[41] The Bu_4N^+ salt of $L_2Ru(NCS)_2$ is assigned as $[(H\text{-}dcbpy^-)_2Ru(NCS)_2](Bu_4N)_2$ and is assumed to be the deprotonated material used in photoelectrochemical cells.[18] When the electron-transfer process is reversible and protons participate in rapidly established acid−base equilibria, a linear dependence of log(base concentration) on the reversible potential is expected (Nernst relationship). Alternatively, if the acid and base forms of $L_2Ru(NCS)_2$ are not in equilibrium on the voltammetric time scale, the peak height of the protonated form will decrease as base is added. Concurrently, an increase in peak height will be observed for the deprotonated form. However, in this nonequilibrium situation, the reversible potentials of both processes will remain unaffected by the base concentration. Cyclic voltammograms obtained at glassy carbon electrodes for solutions of $L_2Ru(NCS)_2$ to which increasing concentrations of $Bu_4N(OH)$ solution were added closely resembled those obtained during the course of reductive bulk electrolysis when deprotonation of $L_2Ru(NCS)_2$ was assumed to occur (Figure 3b−d). Thus, when the number of added equivalents of $Bu_4N(OH)$ was ≥4, cyclic voltammograms were undistinguishable from those obtained over the same negative potential range with bulk electrolyzed solutions (Figure 3d). All these data imply that deprotonated complexes are formed by bulk reductive electrolysis and that protonated and deprotonated forms of $L_2Ru(NCS)_2$ are not in equilibrium on the voltammetric time scale.

The $E^r_{1/2}$ value for the $[(H_{2-x/2}\text{-}dcbpy^{x/2-})_2Ru(NCS)_2]^{x-/(x+1)-}$ redox couple, calculated from deprotonated complex formed by reductive electrolysis, was compared with the values determined for "salts" of $L_2Ru(NCS)_2$ by cyclic voltammetry when more than 3 equiv of $Bu_4N(OH)$ was present. Under these conditions, the voltammetric process of interest is clearly defined, whereas for 2 equiv, a complex response is evident. The results (Figure S1a, Supporting Information) reveal that the $E^r_{1/2}$ value for the first process for solutions of the "salts" is independent of the concentration of $Bu_4N(OH)$, within experimental error, and in agreement with the $E^r_{1/2}$ value determined for the first reduction process of bulk electrolyzed solutions of $L_2Ru(NCS)_2$. This result again confirms that $[(L^{x/2-})_2Ru(NCS)_2]^{x-}$ is not in a rapid acid−base equilibrium with $L_2Ru(NCS)_2$ on the voltammetric time scale and that the same species are formed by bulk electrolysis and direct addition of a strong base.

(g) In Situ Reductive OTTLE Experiments. As noted in the Introduction, electronic spectra are highly indicative of the formation of reduced forms of ruthenium polypyridine compounds. Changes in electronic spectra that occurred during the course of the bulk electrolysis of $L_2Ru(NCS)_2$ were obtained in situ by use of an OTTLE (platinum electrode) experiment. In DMF, $L_2Ru(NCS)_2$ shows (Figure 7) two MLCT bands in the visible region and one dcbpy ligand-based $\pi \rightarrow \pi^*$ transition band in the UV region.[14,27] After a potential of −1.95 V has been applied at 22 °C (Figure 7), all three bands associated with the occurrence of deprotonation are blue-shifted to higher energy (Table 2) and decrease in intensity (Figure 7). No isosbestic points are detected, implying that a range of intermediates may be formed (and reaction pathways occur) during the course of electrolysis. However, the spectrum of the starting solution of

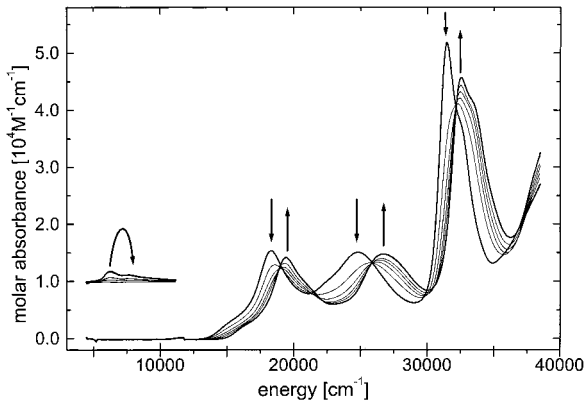

Figure 7. Electronic spectra obtained during the course of OTTLE experiments on the reductive electrolysis of 0.5 mM $L_2Ru(NCS)_2$ in DMF (0.1 M Bu_4NPF_6) at 22 °C; $E_{appl} = -1.95$ V. Inset in the near-infrared region shows additional band observed when experiment is conducted at −58 °C.

$L_2Ru(NCS)_2$ could be quantitatively regenerated (no detectable loss of absorbance) when a 4-fold or greater concentration excess of HBF_4 was added to the electrolyzed solution. When the electrolysis experiment is conducted in the OTTLE cell at −58 °C, an additional band in the near-infrared region is observed at 6300 cm^{-1} (see insert in Figure 7) in initial stages of the electrolysis. Importantly, it was observed that this band collapses prior to exhaustive electrolysis being achieved, so that the final spectrum observed at −58 °C is essentially identical to that recorded for the deprotonated sensitizer at 22 °C. The band at 6300 cm^{-1} is characteristic of formation of the reduced dcbpy ligand and has been found in the electronic spectra of the reduced ester analogue.[20] Thus, at −58 °C, the initial reduction process at platinum electrodes incorporates a step that results in the formation of $[(H_2\text{-}dcbpy^{\bullet-})(H_2\text{-}dcbpy)Ru(NCS)_2]^-$ or $[(H_2\text{-}dcbpy^{\bullet-})_2Ru(NCS)_2]^{2-}$. Hence, at low temperature, the pathway for generation of deprotonated $[(H_{2-x/2}\text{-}dcbpy)_2Ru(NCS)_2]^{x-}$ also involves a homogeneous reaction of reduced $(H_2\text{-}dcbpy)Ru(NCS)_2$ with H^+, H_2O, or $L_2Ru(NCS)_2$. This result proves that homogeneous reaction pathways are available for generation of hydrogen gas.

In other studies,[42,43] the position of the MLCT bands has been correlated with the reversible potentials of the ligand-based reduction and metal-centered oxidation processes. It seems reasonable to assume that this argument can be extended to the comparison of protonated and deprotonated complexes by effectively treating them as a different form of ligand. On this basis, it follows that, since the reversible potential for ligand-based reduction changes by 0.6 V (in the negative direction) and that of metal-based oxidation by only 0.3 V (negative direction, vide infra), deprotonation results in the energy of the ligand π^*-orbitals being increased to a greater extent than the metal d-orbitals. It therefore also follows that the MLCT band, which formally can be assigned to a $Ru(d_\pi)(H_2\text{-}dcbpy(\pi^*)$ transition, increases in energy on deprotonation.

3.2. $L_2Ru(CN)_2$. (a) Voltammetry in DMF. As is the case with $L_2Ru(NCS)_2$, the initial two voltammetric processes for reduction of $L_2Ru(CN)_2$ at a platinum electrode (Figure 8a) were significantly different from that observed when glassy carbon was the electrode material (Figure 8b). If the switching potential in glassy carbon electrode experiments was set before the onset

(41) Streuli, C. A. *Anal. Chem.* **1964**, *36*, 363−369.

(42) Heath, G. A. In *Molecular Electrochemistry of Inorganic, Bioinorganic and Organometallic Compounds*; Pombeiro, A. J. L., McCleverty, J. A., Eds.; Kluwer Academic Publishers: Dordrecht, The Netherlands, 1993; pp 533−547.

(43) Duff, C. M.; Heath, G. A. *Inorg. Chem.* **1991**, *30*, 2528−2535.

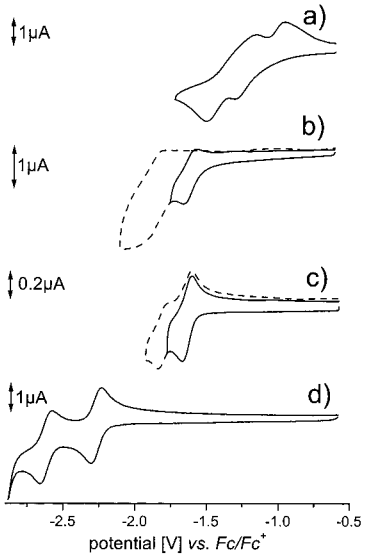

Figure 8. Cyclic voltammograms ($v = 100$ mV s^{-1}) for reduction of $(H_2\text{-dcbpy})_2Ru(CN)_2$. (a) Platinum disk electrode, $c = 1.1$ mM, $T = 25$ °C. (b) Glassy carbon electrode, $c_0 = 1.1$ mM, $T = +25$ °C. (c) Glassy carbon working electrode, $c = 1.1$ mM, $T = -58$ °C. (d) Electrogenerated $[(H_{2-x/2}\text{-dcbpy})^{x/2-})_2Ru(CN)_2]^{x-}$, $c_0 = 1.3$ mM, glassy carbon disk electrode, $T = 25$ °C.

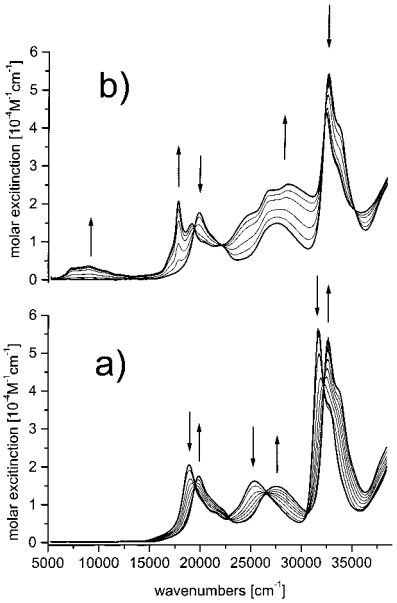

Figure 9. Electronic spectra obtained during the course of OTTLE experiments on the reductive electrolysis of 0.7 mM $(H_2\text{-dcbpy})_2Ru(CN)_2$ in DMF (0.1 M Bu_4NPF_6) at 22 °C. (a) $E_{appl} = -2.0$ V and formation of $[(H_{2-x/2}\text{-dcbpy}^{x/2-})_2Ru(CN)_2]^{x-}$; (b) ligand-based reduction of $[(H_{2-x/2}\text{-dcbpy}^{x/2-})_2Ru(CN)_2]^{x-}$, $E_{appl} = -2.4$ V.

of the second process (−1.8 V), the first process exhibited i_p^{red}/i_p^{ox} values of almost unity for scan rates $v > 1000$ mV s^{-1}, although chemical irreversibility was evident at lower scan rates. This first process also was irreversible when a glassy carbon rotating disk electrode was used at low rotation rates ("log-plots" were nonlinear and had slopes of ≥90 mV). In contrast, at high rotation rates (≥3000 rpm), the first process was close to reversible as slopes of "log-plots" were now 70 ± 5 mV and the $E_{1/2}$ values coincided with values obtained with cyclic voltammetry at high scan rates ($v > 200$ mV s^{-1}). The estimated reversible $E^r_{1/2}$ values for the $[L_2Ru(CN)_2]^{0/-}$ ($T = +25$ °C) couple are given in Table 2 under a range of conditions.

The chemical reversibility of the $L_2Ru(CN)_2$ reduction processes significantly improved when the temperature was lowered to −58 °C. The first process was close to reversible at this temperature under conditions of cyclic, rotating disk, and microdisk electrode voltammetry when glassy carbon electrodes were used. The slopes of "log-plots" (rotating disk and microdisk electrode) confirmed the one-electron nature of the $[L_2Ru(CN)_2]^{0/-}$ process. The second process required higher scan rates ($v >$ 1000 mV s^{-1}) before an i_p^{red}/i_p^{ox} value of unity was approached at −58 °C. The reversible half-wave potential for the $[L_2Ru(CN)_2]^{-/2-}$ process at −58 °C could be calculated from cyclic voltammograms at scan rates $v = 500$ mV s^{-1} and from rotating disk electrode experiments ($f \geq 2000$ rpm). Data obtained under these conditions are summarized in Table 2. Mass-transport-controlled data at the glassy carbon microdisk electrode could not be obtained at −58 °C because of significant adsorption.

(b) Bulk Reductive Electrolysis in DMF. When $L_2Ru(CN)_2$ was reduced by bulk electrolysis at a platinum gauze working electrode using a potential of $E_{appl} = -2.0$ V vs Fc/Fc^+, the formation of H_2 was detected by gas chromatographic analysis of the supernatant gas phase. This result implies that an overall deprotonation reaction occurs in this long time scale experiment, as is the case with reduction of the thiocyanate analogue. After exhaustive electrolysis, the number of electrons per molecule transferred was $n = 3.2 \pm 0.3$. A cyclic voltammogram obtained at a glossy carbon electrode over the negative potential range is shown in Figure 8d. In contrast to the results from measurements made with the protonated form of $(H_2\text{-dcbpy})_2Ru(CN)_2$, both reduction processes of deprotonated $[(H_{2-x}\text{-dcbpy}^{x/2-})_2Ru(CN)_2]^{x-}$ are fully reversible under all voltammetric conditions employed. $E^r_{1/2}$ values calculated from cyclic and near-steady-state microdisk and rotating disk electrode measurements after bulk electrolysis and deprotonation coincided for both processes (Table 2). Slopes of "log-plots" derived from steady-state measurements confirmed that both reduction steps involved one-electron charge-transfer processes.

(c) The Oxidation Process as a Function of Deprotonation. The $E^r_{1/2}$ value for the oxidation of $L_2Ru(CN)_2$ in DMF is readily measured, since the $[L_2Ru(CN)_2]^{0/+}$ process requires only moderately high scan rates ($v \geq 500$ mV s^{-1}) to become fully reversible (Table 2). After exhaustive bulk reductive electrolysis as described above at a platinum electrode, the metal-based oxidation process for deprotonated $(H_2\text{-dcbpy})_2Ru(CN)_2$ is shifted at glassy carbon electrodes to a greater extent negative (0.36 V) than is the case with the thiocyanate analogue (0.30 V). As evidenced by examination of data contained in Table 2, $E^r_{1/2}$ for the $[(H_{2-x}\text{-dcbpy}^{x/2-})_2Ru(CN)_2]^{x-/(x+1)-}$ process is located at +210 mV, which is 360 mV less positive than that found for oxidation of the protonated form. The process for oxidation of deprotonated $L_2Ru(CN)_2$ is followed by a series of complex, possibly surface-based, processes at more positive potentials, similar to those shown for the thiocyanate analogue in Figure 5.

(d) Reductive OTTLE Experiments. The electronic spectra obtained during reductive electrolysis ($E_{appl} = -2.0$ V) and deprotonation of $(H_2\text{-dcbpy})_2Ru(CN)_2$ were monitored with an OTTLE cell arrangement (platinum working electrode) to give the result presented in Figure 9a. No isosbestic points were observed, and the absorption bands of $[(H_{2-x/2}\text{-dcbpy}^{x/2-})_2Ru(CN)_2]^{x-}$ are shifted to higher energy and have a smaller extinction coefficient compared to those of $(H_2\text{-dcbpy})_2Ru(CN)_2$. All these electronic spectral data imply that the energy gap between the ruthenium d-orbitals and the ligand π^*-orbital has increased, as also predicted on the basis of voltammetric data.

The result of an OTTLE electrolysis experiment on deprotonated $(H_2\text{-dcbpy})_2Ru(CN)_2$ at a potential more negative than the first reduction process of deprotonated $[(H_{2-x/2}\text{-dcbpy}^{x/2-})_2Ru(CN)_2]^{x-}$ ($E_{appl} = -2.4$ V) is shown in Figure 9b. In this case, exhaustive electrolysis could never be achieved (zero current not attained). Instead, a steady-state condition was attained which produced the electronic spectrum shown in Figure 9b. The spectrum obtained after reduction of the deprotonated complex indicates that a dcbpy ligand-based reduction process has occurred, since it resembles that of the one-electron reduced form of the ester analogue ($[(Et_2\text{-dcbpy})_2Ru(CN)_2]^-$).[20] The NIR absorption band at 8000 cm^{-1} is expected for a bpy-type ligand-based reduction process.[44,45] This band is assigned to an intraligand $\pi_1^* \rightarrow \pi_2^*$ transition[20] of the reduced dcbpy ligand but occurs at higher energies than for the ester analogue ($\sim$6000 cm^{-1}), which again highlights the altered electronic environment of the ligand caused by deprotonation. The occurrence of four isosbestic points in this OTTLE experiment is also noteworthy, as is the fact that the electronic spectrum of the starting solution ($[(H_{2-x/2}\text{-dcbpy}^{x/2-})_2Ru(CN)_2]^{x-}$) could be quantitatively regenerated by electrochemical oxidation ($E_{appl} = -1.0$ V).

As observed with $[(H_{2-x/2}\text{-dcbpy}^{x/2-})_2Ru(NCS)_2]^{x-}$, no rapid spectral changes could be detected when the applied potential was set to a very negative value of -2.7 V, which is more negative than the reversible potential for the second reduction process. Rather, after prolonged electrolysis time ($t > 30$ min), decomposition was observed, and irreversible spectral changes occurred, as evidenced by the loss of isosbestic points.

(e) Bu_4N^+ "Salts" of $L_2Ru(CN)_2$. Bu_4N^+ salts of known stoichiometry were prepared (see Experimental Section). The reversible reduction potentials for Bu_4N^+ salts were measured over a range of 2−20 equiv of $Bu_4N(OH)$. Similarly, as found for the thiocyanate analogue, the $E^r_{1/2}$ value for this process is independent of hydroxide concentration over this range and coincides with the value obtained from electrochemically generated $[(H_{2-x/2}\text{-dcbpy}^{x/2-})Ru(CN)_2]^{x-}$ (Figure S1b, Supporting Information).

4. Conclusions

4.1. Summary. The reversible potentials for the ligand-based $[(H_2\text{-dcbpy})_2RuX_2]^{0/-}$ and $[(H_2\text{-dcbpy})_2RuX_2]^{-/2-}$ reduction processes have been determined in DMF. Short time domains, reduced temperatures, and glassy carbon electrodes are required in order to obtain chemically and electrochemically reversible responses for all processes under voltammetric conditions. At platinum electrodes, the reduction of both compounds is considerably more complex than that at glassy carbon. Data suggest that this complexity is associated with the much lower overpotential for hydrogen ion reduction to hydrogen gas at platinum relative to glassy carbon electrodes. Reduction under long time scale conditions of bulk electrolysis resulted in overall deprotonation and formation of molecular hydrogen at platinum electrodes. However, partial rather than complete deprotonation of $(H_2\text{-dcbpy})_2RuX_2$ occurs, as established from the number of electrons transferred in bulk electrolysis experiments. Spectroscopic data and voltammetric studies undertaken in the presence of deliberately added acid or base imply that the number of protons removed is of the order of two. This number is supported by comparison of data obtained from molecular orbital calculations and measured reversible potentials for reduction of protonated and deprotonated forms of $(H_2\text{-dcbpy})_2Ru(NCS)_2$, which suggests that $[(H\text{-dcbpy}^-)_2RuX_2]^{2-}$ is formed by reductive electrolysis of $(H_2\text{-dcbpy})_2RuX_2$.

4.2. Relationship of Results to Photovoltaic Cells. The potential for the first reduction process is shifted by 0.65 V (more negative) when deprotonated $[(H_{2-x/2}\text{-dcbpy}^{x/2-})_2RuX_2]^{x-}$ is formed. In contrast, the reversible potential for the oxidation of deprotonated complexes is only shifted by about 0.3 V. Scheme 1 suggests that no enhanced cell performance is expected if the reversible potential for the oxidation of the sensitizer is lowered, as occurs upon deprotonation. Indeed, the thermodynamic driving force required for the dye regeneration by the electrolyte ion, I^-, will decrease. The increased performance of deprotonated forms of the sensitizer in photovoltaic cells is therefore likely to be a result of considerations not associated with dark potentials. For example, band potentials of nanosized TiO_2 semiconductor electrodes are very sensitive toward the solution environment and can shift dramatically when small changes are made to the electrolyte counterions present in the solution phase.[40,46−48] A related effect also may apply if the TiO_2 semiconductor band potentials shift when sensitizers containing different levels of deprotonation and types of counterions are used. Alternatively, the addition of base to TiO_2 photovoltaic cells may also lead to deprotonation of TiO_2 surface hydroxyl groups[49] and thus will result in a change of surface states, which in turn may have dramatic effects on the overall performance of the solar cell device.

Electronic spectra obtained during the course of reductive electrolysis reveal that deprotonation also leads to the MLCT bands being shifted toward the UV region and that lowering of the extinction coefficient also occurs. These features would normally be expected to lead to poorer performance when deprotonated forms of L_2RuX_2 are used as sensitizers in photovoltaic cells. Interestingly, deprotonated forms of the $L_2Ru(NCS)_2$ sensitizer are commonly employed in TiO_2 photoelectrochemical cells and found to exhibit higher energy conversion efficiencies[18] than the protonated form. On the basis of our findings, the explanation for this improved performance must be related to changes in thermodynamics or kinetics rather than spectral properties, because we conclude that the deprotonation causes the light-harvesting MLCT bands to be shifted toward the UV region and also decrease in absorbance, and we note that both features are generally considered to be detrimental to conversion efficiencies.[50]

As a further source of explanation, consideration must be given to the initial electron excitation and injection processes. Reports on the binding mode of L_2RuX_2 onto the TiO_2 surface[7,9−11] suggest that predominantly ester formation with TiO_2 and two carboxylic acids on one H_2-dcbpy ligand occurs, whereas the other two carbon acid groups, located on the second H_2-dcbpy ligand, are available for interaction with solvent. If the latter two acid groups are deprotonated, the LUMO of the H_2-dcbpy ligand not attached to the TiO_2 surface will significantly rise in energy compared to the other H_2-dcbpy ligand. The absorption spectrum of the complex will then consist of transitions into the TiO_2 attached and deprotonated bipyridine moiety. This is advantageous, since it broadens the absorption bands and increases the light-harvesting spectrum

(44) Coombe, V. T.; Heath, G. A.; MacKenzie, A. J.; Yellowlees, L. J. *Inorg. Chem.* **1984**, *23*, 3423−3425.
(45) Heath, G. A.; Yellowlees, L. J.; Braterman, P. S. *J. Chem. Soc., Chem. Commun.* **1981**, 287−289.
(46) Wolfbauer, G.; Bond, A. M.; Eklund, J. C.; MacFarlane, D. R. *Sol. Energy Mater. Sol. Cells* **1999**, submitted.
(47) Enright, B.; Redmond, G.; Fitzmaurice, D. *J. Phys. Chem.* **1994**.
(48) Wolfbauer, G. Ph.D. Thesis, Monash University, Melbourne, Australia, 1999.
(49) Kokubo, T. *Thermochim. Acta* **1996**, *280*, 479−490.
(50) Kalyanasundaram, K.; Grätzel, M. *Coord. Chem. Rev.* **1998**, *177*, 347−414.

of the sensitizer. Electron injection from the TiO_2-attached ligand into the TiO_2 occurs on the subpicosecond time scale[51] due to the good orbital overlap between the TiO_2 manifold and H_2-dcbpy ligand.[50,52] However, it has been shown that direct linkage of the chromophore with the semiconductor is not necessary for efficient electron injection.[53,54] Thus, the electron injection into the TiO_2 from the non-surface-attached ligand occurs either directly or by an electron cascading effect via the π^*-orbital of the surface-attached ligand.[53] A more recent study,[28] employing crystallographic data and molecular modeling, confirms the possibility of surface attachment via two acid groups but suggests that, for steric reasons, these two acid groups are located on different bipyridine ligands. Each dcbpy ligand can then use one carboxylate to form an ester linkage with the TiO_2 surface, leaving the second carboxylate group in either the protonated or deprotonated form. Similar considerations apply as pointed out above: deprotonation of the remaining two acid groups leads to a broadening of the MLCT bands. Importantly, in this case, a direct pathway exists for electrons promoted into the π^*-orbitals of the deprotonated 4-carboxypyridine ring to cascade into the TiO_2 conduction band, thereby improving the light-harvesting properties of the sensitizer.

Quantitative knowledge concerning the shift of redox potentials upon deprotonation offers the exciting possibility of being able to tune the redox potentials and MLCT bands to a desired value but also implies that great care has to be taken in studies on L_2RuX_2 complexes, whether attached to semiconductor surfaces or not, to ensure that a known and stable degree of protonation is maintained throughout the experiments.

Acknowledgment. G.W. acknowledges financial support provided from a Monash Graduate Scholarship and a Monash Publication Award.

Supporting Information Available: Detailed description of the instrumentation, methods, reagents, and compounds used; plot of $Bu_4N(OH)$ concentration versus the reversible half-wave potential for the reduction process of $[(H_{2-x/2}\text{-dcbpy})^{x/2-})_2\text{-}RuX_2]^{x-}$ (Figure S1) (PDF). This material is available free of charge via the Internet at http://pubs.acs.org.

JA992402G

(51) Ellingson, R. J.; Asbury, J. B.; Ferrere, S.; Ghosh, H. N.; Sprague, J. R.; Lian, T. Q.; Nozik, A. J. *J. Phys. Chem. B* **1998**, *102*, 6455−6458.
(52) Moser, J. E.; Bonnote, P.; Grätzel, M. *Coord. Chem. Rev.* **1998**, *171*, 245−250.
(53) Argazzi, R.; Bignozzi, C. A.; Heimer, T. A.; Meyer, G. J. *Inorg. Chem.* **1997**, *36*, 2−3.
(54) Heimer, T. A.; Darcangelis, S. T.; Farzad, F.; Stipkala, J. M.; Meyer, G. J. *Inorg. Chem.* **1996**, *35*, 5319−5324.